Title: Revisiting properties of CaCoSinO2n+2. Crystal and electronic structure

Author: Magdalena Szubka, Paweł Zajdel, Marcin Fijałkowski, Ewa Talik, A. Balerna, M. Cestelli-Guidi [i in.]

Citation style: Szubka Magdalena, Zajdel Paweł, Fijałkowski Marcin, Talik Ewa, Balerna A., Cestelli-Guidi M. [i in.]. (2022). Revisiting properties of CaCoSinO2n+2. Crystal and electronic structure. "Journal of Magnetism and Magnetic Materials" (2022), Vol. 546, art. no. 168858, s. 1-8.
DOI: 10.1016/j.jmmm.2021.168858

Journal of Magnetism and Magnetic Materials 546 (2022) 168858

Contents lists available at ScienceDirect

Journal of Magnetism and Magnetic Materials

journal homepage: www.elsevier.com/locate/jmmm

Revisiting properties of $CaCoSi_nO_{2n+2}$. Crystal and electronic structure

M. Szubka [a,*], P. Zajdel [a], M. Fijałkowski [a], E. Talik [a], A. Balerna [b], M. Cestelli-Guidi [b], M. Romani [b], J. Łażewski [c], P.T. Jochym [c]

[a] Institute of Physics, University of Silesia, ul. 75 Pułku Piechoty 1, PL-41-500 Chorzów, Poland
[b] Lab. DAFNE-Light, INFN-LNF, Via E. Fermi 40, Frascati I-00044, Italy
[c] Institute of Nuclear Physics, PAS, ul. Radzikowskiego 152, PL-31-342 Kraków, Poland

ARTICLE INFO

Keywords:
Pyroxenes
XAS
XRD
XPS
DFT
SEM

ABSTRACT

In a public space there are several reports of materials with general stoichiometry $CaCoSi_nO_{2n+2}$. Pyroxene $CaCoSi_2O_6$ is probably the best-known representative for n = 2 but not much is known about materials with n = 3 and n = 4. In this study, attempts were carried out to synthesize those phantom materials and it was found that they do not exist as a single phase. A quantitative XRD analysis revealed that their chemical composition is correct but the formula should be written as $CaCoSi_2O_6$ + (n-2)SiO_2. Similar qualitative conclusions were drawn from investigation of magnetic (DC magnetometry) and electronic properties using X-ray Photoelectron Spectroscopy (XPS) and Si K edge X-ray Absorption Spectroscopy (XAS). Additionally, the DFT ab initio calculations were carried out to obtain electronic signature from band structure of $CaCoSi_2O_6$.

The apparent influence of the excess of SiO_2 on magnetic properties of this "series" can be understood in terms of presence and suppression of secondary phases like $Ca_2CoSi_2O_7$, which form when the starting materials are not homogenized properly. Addition of surplus SiO_2 suppresses their formation leaving clear signature from $CaCoSi_2O_6$, which also can be synthesized from stoichiometric mixture using proper techniques.

1. Introduction

Continuous use of cobalt-based pigments dates since thousands of years ago [1]. They are being commonly used in the ceramic industry as blue glazes and for bulk coloration of unglazed porcelain stoneware [2]. Their colors depend on ligand coordination of the ion in the host lattice. If cobalt 2+ is in tetrahedral coordination, the color is deep blue [3] while, if it is surrounded by six or eight atoms of oxygen the hue shifts to pink or violet [4]. In case of glasses and many crystal structures Co^{2+} exists in the tetrahedral coordination, but in case of $CaCoSi_nO_{2(n+1)}$ ceramic, it does occupy the octahedral or cubic site. Cobalt based phases with increased silica content like $CaCoSi_nO_{2(n+1)}$ are interesting candidates for ceramic colorants, since they possess smaller amount of potentially toxic cobalt as compared to the commonly used Co-olivine Co_2SiO_4 and spinel $CoAl_2O_4$. The second equally important factor is the increasing price of cobalt [5], which only in 2021 went up from about 33 k$ per ton up to 53 k$ [6]. A free patent available on-line [7] claims rights to a series of compounds between "$CaCoSi_2O_6$ and $CaCoSi_6O_{14}$" with $CaCoSi_3O_8$ listed as the stoichiometric composition with "the highest color saturation". Although the term "stoichiometric composition" does not imply crystallinity, it suggests the existence of phases with general stoichiometry $CaCoSi_nO_{2n+2}$. For n = 2 it is a known pyroxene $CaCoSi_2O_6$ [8,9], however, not much is known about materials with n = 3 and n = 4, which seem to be analogous to known pigments $CaCuSi_nO_{2n+2}$.

The copper-based pigments were identified already by Humphrey Davy [1] but the actual compositions for Han Purple $BaCuSi_2O_6$, Han Blue $BaCuSi_4O_{10}$ or Egyptian Blue $CaCuSi_4O_{10}$ were established later [10,11]. Recently $CaCuSi_4O_{10}$ has been considered as possible new material for a near-infrared emission purposes due to its high yield and an excellent structural stability [12]. It has been noticed, that the stability is mostly confined within layers, which makes the system liable to exfoliation [13,14] and thus nanofabrication.

At the same time, cobalt based materials, which were also mentioned in Davy's lecture [1] are less common. Recently, most attention was devoted to alkali earth rich phases $A_2CoSi_2O_7$ (A = Ca, Sr, Ba) [15,16,17]. The Ca-material displays type-II multiferroicity generated by an incommensurate magnetic order at low temperatures and Sr one is an example of p-d driven magnetoelectric coupling, which persists even in a paramagnetic state similar to $Ba_2CoGe_2O_7$ [18]. Only one stable

* Corresponding author.
E-mail address: magdalena.szubka@us.edu.pl (M. Szubka).

https://doi.org/10.1016/j.jmmm.2021.168858
Received 6 August 2021; Received in revised form 10 November 2021; Accepted 16 November 2021
Available online 26 November 2021

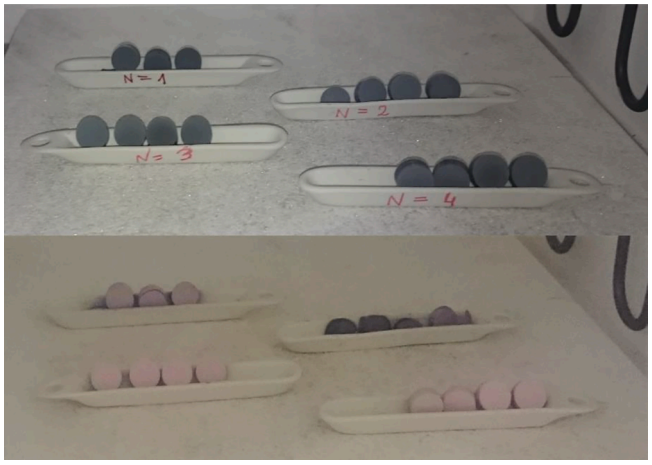

Fig. 1. Photograph of the samples before (top) and after (bottom) the first synthesis at 1150 °C. Samples from top to bottom - N1H to N4H.

member of $CaCoSi_nO_{2(n+1)}$ series has been reported in literature, a pyroxene $CaCoSi_2O_6$ [8,9,19] with a handful of other isostructural compounds crystallizing in *C*2/*c* space group: $CaFeSi_2O_6$, $CaNiGe_2O_6$, $CaCoGe_2O_6$ and $CaMnGe_2O_6$ [20].

In this work, an attempt to synthesize the cobalt-based materials with n = 3 and n = 4 was carried out together with establishing an experimental protocol for a synthesis of pure phase material with n = 2.

2. Materials and methods

Polycrystalline samples with nominal stoichiometry $CaCoSi_nO_{2(n+1)}$ n = 2, 3, 4 (called later on N2H, N3H, N4H) were synthesized using ceramic method in the following way. Stoichiometric amounts of $CaCO_3$ (Sigma-Aldrich, >99.0% C4830-100G), Co_3O_4 powder (Sigma-Aldrich, 221643-50G) and fused (amorphous) silica (Sigma-Aldrich, >99.9%, 342831-100G) in quantity appropriate for 2 g of the final products were mixed together in a planetary ball mill for 2 h at 350 rpm. The powders were removed from the cell using acetone, dried and pelletized in a 10 mm pressure die into several discs, each around 1 mm thick. Starting materials were gray with N3H, N4H samples being visibly brighter. The discs were placed in Al_2O_3 based boats in a chamber furnace. The furnace proceeded the following program: ramp to 850 °C in 3 h, dwell 2 h, ramp to the final temperature 1150 °C in 1 h, dwell 48 h, cool down to room temperature. The first stop around 850 °C served two purposes. It allowed the carbonate to decompose into oxide as well as to reduce Co_3O_4 into CoO [21]. Omitting this step causes formation of Co_2SiO_4 [22], which is impossible to remove by subsequent reheatings.

After heating at 1150 °C the N3H and N4H specimens were bright pink and n = 2 slightly blue with visible signs of glazing of the pellet (Fig. 1). This led to the conclusion that the n = 2 material might have been close to its melting point. The partially glazed n = 2 sample N2H was rejected from further analysis.

After that a new synthesis for n = 2 was carried out at a lower temperature of 1100 °C. The obtained sample was pink with slight blueish hue, without glassy surface. This sample is referred as the N2L (htx1). After the first heating, the pellets were again ground in a planetary mill. A second round of pelletizing and reheating was carried out and after that, sample N2L lost its blue hue. No signs of glazing were observed. Samples (N3H, N2L) after the second heating were marked htx2.

Room temperature x-ray diffraction measurements (XRDs) were carried out on a Philips PW1050 diffractometer in Bragg-Brentano geometry using Ni-filtered Cu K source operating at 30 kV/30 mA. The diffractograms were collected in step mode from 7° to 135°, with step size 0.02°, time per step 12 s. Rietveld refinement were carried out using Fullprof Program Suite [23]. The samples were finely powdered and deposited on a double-sided sticky tape which was later attached to a glass slide.

Bulk magnetization measurements were performed in a rso-mode using Quantum Design MPMS system in the Institute of Physics University of Silesia, Katowice, Poland. Samples were cooled down from room temperature (RT) down to 2 K. Then an external magnetic field $\mu_B H$ = 0.01 T was applied and a Zero Field Cooling (ZFC) run was collected on warming up. Then, samples were cooled down again without switching the field off and the Field Cooled (FC) data were collected up to 350 K.

The microstructural observations and the microcompositional analyses were conducted using the JEOL-7600F scanning electron microscopy (SEM) equipped with the Oxford X–ray energy dispersive spectroscopy (EDS) microprobe. Microprobe operated at 15 kV accelerating voltage and 1 nA probe current. The samples were coated with a thin layer of gold to avoid charging effects. High resolution SEM images were obtained using an extra-lens Everhart-Thornley secondary electron detector (LEI). The pictures were acquired at an accelerating voltage of 5–10 kV and probe current of 200 pA.

X-ray photoemission spectra were collected using a PHI5700/660 Physical Electronics Photoelectron Spectrometer with monochromatic Al K_α X–ray radiation (1486.6 eV). The energy of the electrons was measured with a hemispherical analyzer and resolution of about 0.3 eV. The measures of photoelectron emission were taken from a surface area with a diameter of 800 μm and at take-off angle 45°. The binding energy was determined with reference to the C 1s component set at 285 eV. The quantification of XPS spectra using the peak area and peak height sensitivity factor used to the Multipak Physical Electronics application. The XPS core level spectra were fitted using the Doniach-Sunjic method [24].

XANES studies were performed in transmission mode on the DXR-1 [25] Beamline at the DAΦNE-Light Laboratory [26] using the 510 MeV e- e+ storage ring in operation at the INFN, Frascati. Materials were finely powdered in an agate mortar. For measurements of the Si K edge samples were suspended in Apiezon M before being deposited on a thin paper (Schleicher&Schuell Optical paper). The amount of sample and its thickness were adjusted experimentally on several specimens to obtain acceptable signal to noise ratios. Apiezon M has minimal SiO_2 contribution (edge step 0.02), which is negligible with the overall step for all tested samples (>1.0). The XANES at the Si K edge were recorded for the energy range 1828–1873 eV with a 0.15 eV step. In order to perform the energy scale calibration, a ground silicon wafer was used. The position of the edge E_0 = 1839.9 eV agrees well with the value from the XRD [27].

3. Results and discussion

3.1. XRD

Rietveld refinement [28] showed that only 4 phases were necessary to account for reflections in all of the samples: a monoclinic $CaCoSi_2O_6$ (SG *C*2/*c*), a tetragonal $Ca_2CoSi_2O_7$ (SG *P*-42$_1$*m*), a trigonal quartz SiO_2 (SG *P*3$_2$21, t-SiO_2) and a tetragonal cristobalite SiO_2 (SG *F*4$_1$2$_1$2, c-SiO_2). After the first heating, the sample N2L revealed only presence of two phases $CaCoSi_2O_6$ and $Ca_2CoSi_2O_7$. Samples N3H and N4H had only $CaCoSi_2O_6$ and two polymorphs of SiO_2.

A semi-quantitative (no microabsorption correction) analysis of weight percentage ratio for the samples gave the following results after the first heating:

a) N2L htx1: 94.0% $CaCoSi_2O_6$ + 5.5% $Ca_2CoSi_2O_7$ + 0.5% SiO_2,
b) N3H htx1: 79.0% $CaCoSi_2O_6$ + 0.1% $Ca_2CoSi_2O_7$ + 20.9% SiO_2,
c) N4H htx1: 65.0% $CaCoSi_2O_6$ + 0.0% $Ca_2CoSi_2O_7$ + 35.0% SiO_2.

In the first case, the crystalline SiO_2 content refined to 0.5%. The

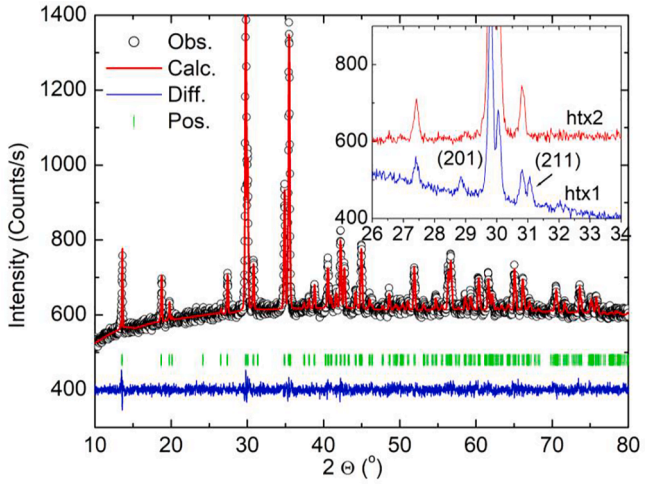

Fig. 2. XRD of sample N2L after the second heating. Tick marks indicate possible positions for reflections of $CaCoSi_2O_6$. The inset presents suppression of the $Ca_2CoSi_2O_7$ phase in the second heating as seen by (201) and (211) reflections.

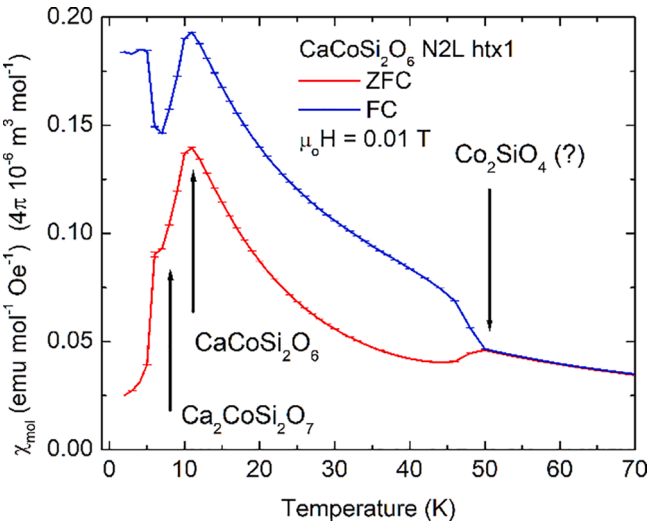

Fig. 3. Molar susceptibility (per mol of Co) for sample N2L after the first heating (htx1).

weight percentages obtained for $Ca_2CoSi_2O_7$ in cases b) and c) were equal 0.0 within 3σ and practically meant that it was not present in the samples. The presence of 5.5% of $Ca_2CoSi_2O_7$ in sample N2L explained its slight blue hue as compared to N3H and N4H.

The XRD analyzes for samples after the second heating (htx2) gave the following semi-quantitative weight percentages (Fig. 2):

a) N2L: 100% $CaCoSi_2O_6$,
b) N3H: 79.9% $CaCoSi_2O_6$ + 0.1% $Ca_2CoSi_2O_7$ + 20.0% SiO_2.

A comparison with results obtained after the first heating clearly showed that the $CaCoSi_2O_6$ was the dominant phase and the additional heating round suppressed the $Ca_2CoSi_2O_7$ content to 0, within uncertainty of refinement. In case of sample N3H, the reheating did not change the amount of excess SiO_2 but almost completely converted it to the tetragonal phase. For sample N3H, the total mass ratio of $CaCoSi_2O_6$:SiO_2 (normalized to 100% and assuming no $Ca_2CoSi_2O_7$) was found to be equal to 80:20. This is equivalent to a molar ratio $CaCoSi_2O_6$:SiO_2 of 1:1.05(5), which is in agreement with nominal stoichiometry 1:1 for

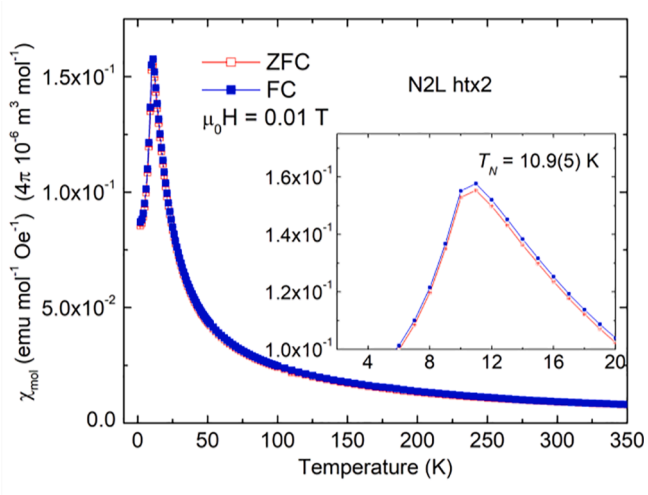

Fig. 4. Molar susceptibility (per mol of Co) for sample N2L after the second heating (htx2). The inset expands region close to the transition temperature.

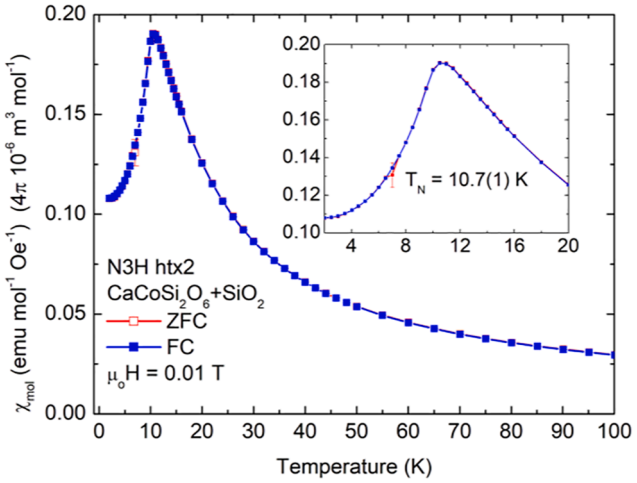

Fig. 5. Molar susceptibility for sample N3H after the second heating (htx2). The inset expands region close to the transition temperature.

$CaCoSi_3O_8$.

Similar analysis for sample N4H (after only 1 round of heating) gave a molar ratio $CaCoSi_2O_6$:SiO_2 1:2.25(5) which is elevated but close to the nominal 1:2 for $CaCoSi_4O_{10}$. The elevated value is caused by omitting the microabsorption correction which boosts phases with lower absorption coefficients.

The final lattice parameters at room temperature obtained for N2L (htx2) sample were a = 9.8017(2) Å, b = 8.9616(2) Å, c = 5.2456(1) Å, β = 105.436(2)° and are in agreement with those published earlier by Ghose and Durand [9,19]. Atomic parameters obtained using Rietveld method were found to be: a common isotropic displacement parameter B_{iso} = 1.05(5) and atomic positions Co (0, 0.9065(6), 0.25), Ca (0, 0.2945(6), 0.25), Si (0.2885(5), 0.0890(7), 0.2313(10)), O1 (0.1155(8), 0.0985(13), 1.1544(15)), O2 (0.3549(10), 0.2440(11), 0.3182(20)), O3 (0.3536(8), 0.0172(9), −0.0118(30)). Conventional Rietveld agreement factors were R_p = 1.0%, R_{wp} = 1.28, R_{exp} = 1.17, χ^2 = 1.21.

3.2. Magnetization

The magnetization of N2L sample was measured after both heatings (labeled htx1 and htx2). This - measured after the first heating (htx1) - is

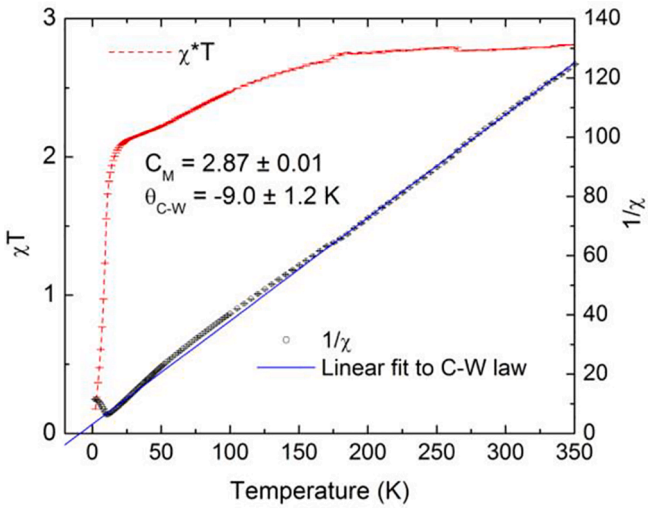

Fig. 6. Curie-Weiss fits to the low temperature data. Black line – Method 1 (linear regression with weights). Blue line – Method 2 – non-linear simplex fit.

presented in the Fig. 3 and differences between ZFC and FC runs clearly revealed transitions coming from $Ca_2CoSi_2O_7$, $CaCoSi_2O_6$ and possibly Co_2SiO_4 [29]. The presence of Co_2SiO_4 has not been detected by the XRD. The same material, after the second heating (htx2), displayed only one transition at 11 K (Fig. 4) confirming phase purity indicated by the XRD.

Magnetization of sample N3H after the second heating was recorded in a narrower temperature range from 2 K to 100 K. In order to normalize the data per mol of Co. The nominal molar mass of $CaCoSi_3O_8$ 311.26 g/mol was used and the excess of SiO_2 was treated as nonmagnetic. This approximation is equivalent to equi-molar contributions of 1 $CaCoSi_2O_6$ + 1 SiO_2 and is in good agreement with the XRD result (1:1.05(5)). The molar susceptibility (per mol of Co) is presented in Fig. 5. Linear Curie-Weiss fits to the inverse of magnetic susceptibility between 200 K and 350 K gave molar Curie constant of $C_M = 2.8611(2)$ and paramagnetic Curie-Weiss temperature of $\theta_{CW} = -8.21(3)$ K (Fig. 6). The value of the Curie constant points towards a high-spin Co^{2+} configuration and the negative C-W temperature agrees with an overall antiferromagnetic character of the magnetic signal.

3.3. SEM

The morphology of the synthesized ceramics was analyzed by SEM equipped with the energy dispersive spectrometry EDS. Examples of the secondary electron images of the $CaCoSi_nO_{2n+1}$ ceramics at magnification 10 000x and the elemental analysis of the $CaCoSi_2O_6$ sample are shown in Fig. 7. Microscopic observation showed the homogenous

Table 1
Chemical composition for $CaCoSi_nO_{2(n+1)}$ ceramics, determined from XPS and EDS measurements.

	Chemical composition			
$CaCoSi_nO_{2(n+1)}$ ceramics	**Ca**	**Co**	**Si**	**O**
N2L (XPS)	1.0	1.0	2.0	6.0
N2L (SEM/EDS)	1.0	1.0	2.0	10.0
N3H (XPS)	0.9	1.0	3.3	9.2
N3H (SEM/EDS)	1.3	1.0	3.3	18.4

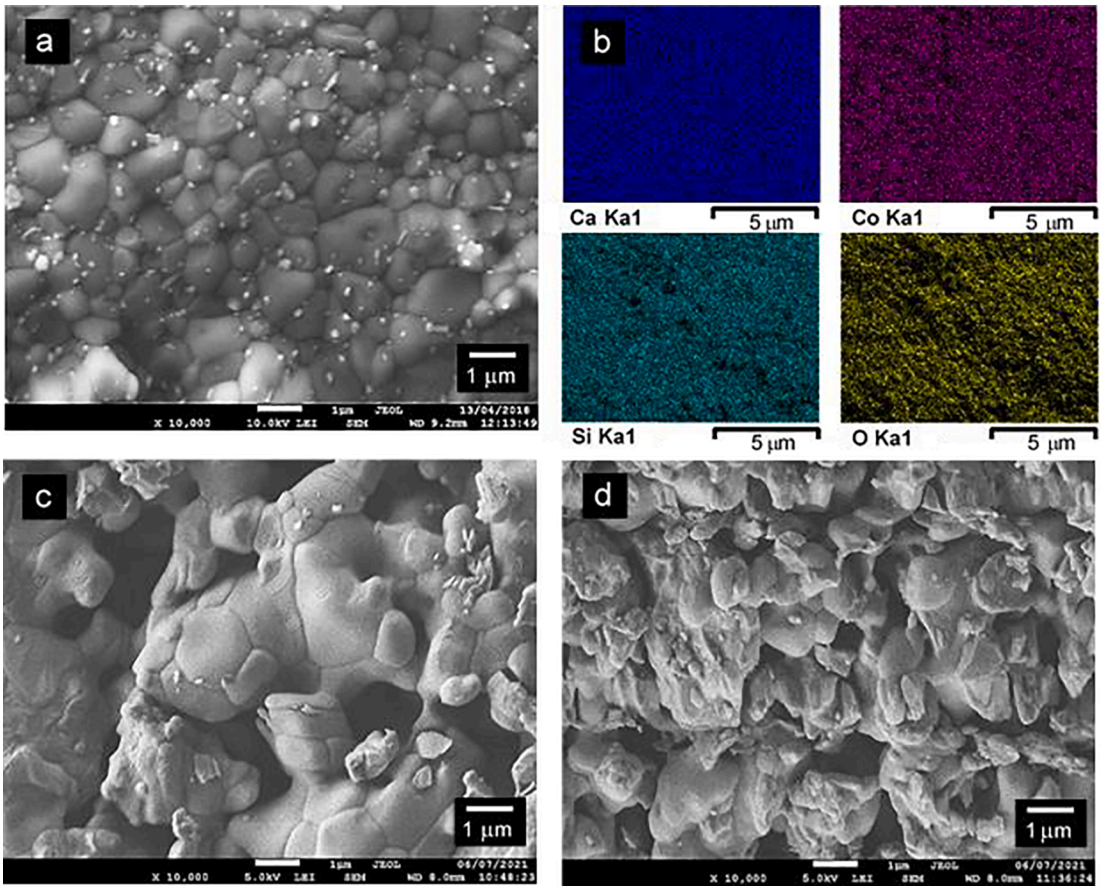

Fig. 7. SEM images at the same magnifications for $CaCoSi_nO_{2(n+1)}$ ceramics: a) N2L (htx2) with b) EDS element mapping of Ca, Co, Si and O, c) N3H (htx2) and d) N4H (htx1).

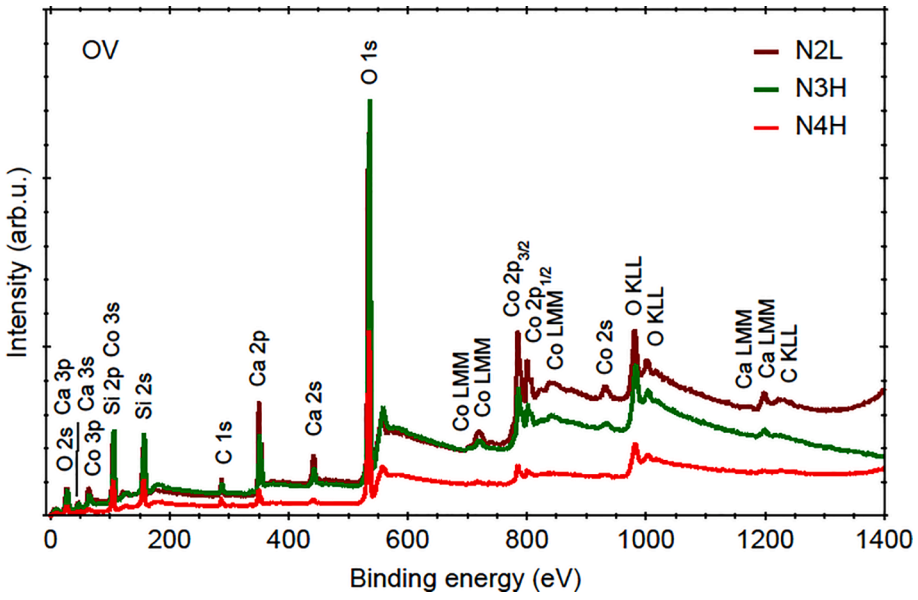

Fig. 8. The XPS spectra of the $CaCoSi_nO_{2(n+1)}$ ceramics: N2L (htx2), N3H (htx2) and N4H (htx1) in the wide energy range 0–1400 eV.

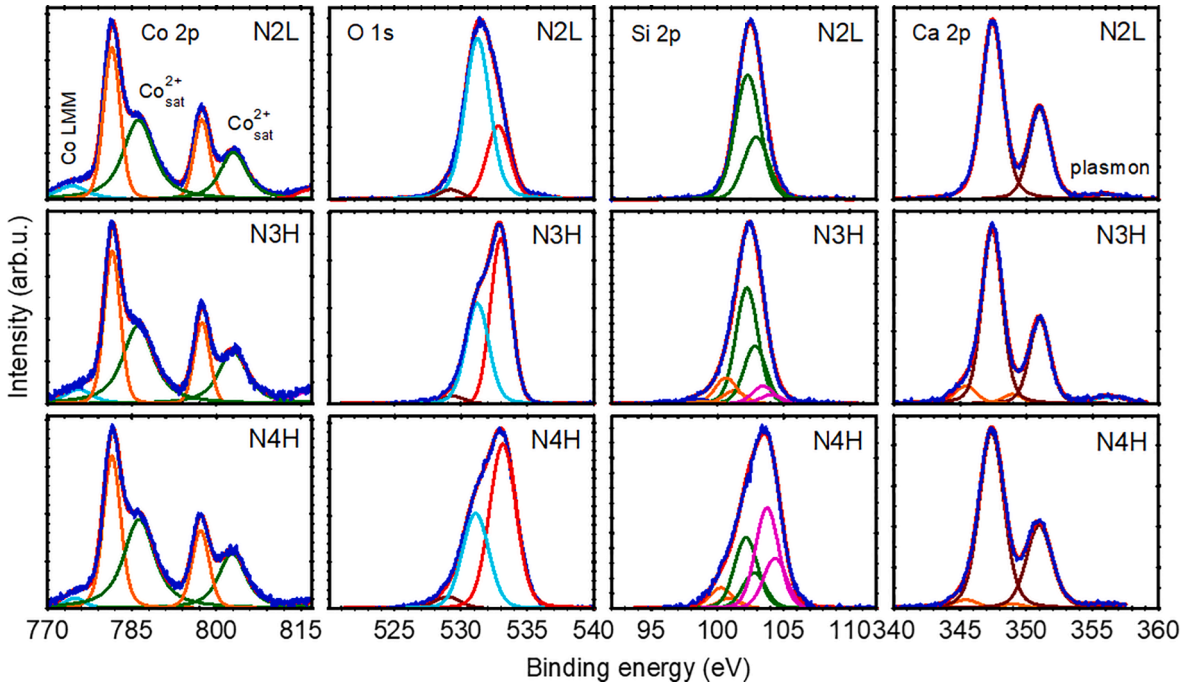

Fig. 9. A high-resolution photoemission spectra of Co 2p, O 1s, Si 2p and Ca 2p for $CaCoSi_nO_{2(n+1)}$ ceramics: N2L (htx2), N3H (htx2) and N4H (htx1).

distribution of compound's elements and not regular shape of pigment molecules which are partially agglomerated. The microanalyses presented in Table 1 showed a chemical composition close to the nominal one for all investigated samples.

3.4. XPS

Fig. 8 shows XPS spectra in the wide energy range 0–1400 eV of the UHV-cleaved examined ceramics. Apart from the lines representing compound's elements no contaminations were found, except for carbon. The existence of some carbon contamination can be caused by the incomplete removal of organic impurities or sample preparation. The atomic concentrations of $CaCoSi_nO_{2n+1}$ ceramics were calculated based on the ratio of each of the components to the sum of all compound's elements with the detection level equals to 0.1%. The chemical composition of $CaCoSi_nO_{2n+1}$ ceramic samples (shown in Table 1) confirmed proper stoichiometry of the compounds. Identified excess of oxygen can be explained similarly to the case of carbon. These results confirm the ceramic compositions determined from the EDS spectra.

The core level X-ray photoelectron lines of Co 2p, O 1s, Si 2p and Ca 2p were deconvoluted after background subtraction and shown in Fig. 9. Based on the Co 2p spectra properties the possible Co oxidation state variations can be estimated. The Co 2p lines consist of two peaks which represent to their angular momentum of electrons. The characteristic value of binding energy for Co $2p_{3/2}$ line equals 781.4 eV and 797.4 eV for Co $2p_{5/2}$ line with spin–orbit splitting approximately equal to 16 eV and strong shake-up satellite peaks located approximately 6 eV above the Co 2p main peaks confirmed divalent oxidation state of Co cation

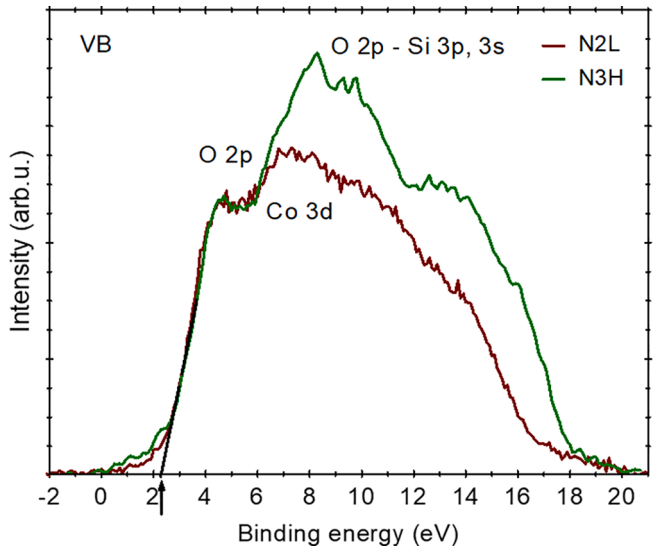

Fig. 10. Valence bands for $CaCoSi_nO_{2(n+1)}$ ceramics: N2L (htx2), N3H (htx2).

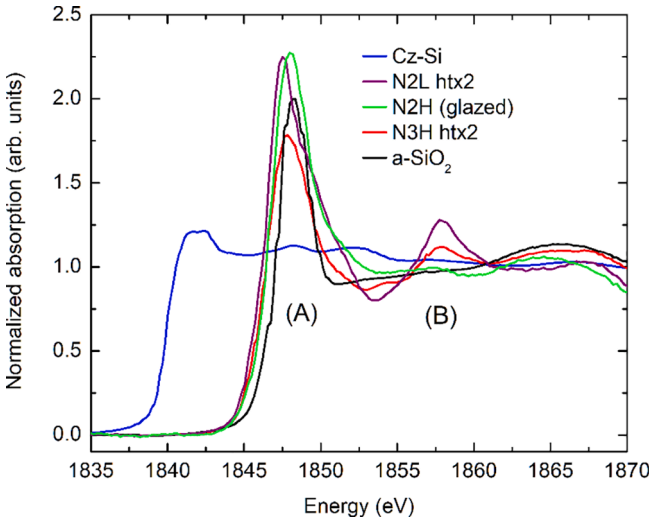

Fig. 11. Normalized Si K absorption edges of the $CaCoSi_2O_6$ (N2L htx2), $CaCoSi_3O_8$ (N3H htx2) plotted against standard materials amorphous SiO_2 (a-SiO_2) and silicon grown using Czochralski method (Cz-Si).

characteristic for bulk of $CaCoSi_nO_{2n+1}$ ceramics [30,31]. Moreover, the satellite peaks registered at about 6 eV above Co 2p main lines can be linked to the high-spin states of Co^{2+} species. Unfortunately, the splitting of satellite peaks of Co^{2+} is similar for divalent cobalt in octahedral and tetrahedral coordination [30].

Such result is not surprising. Petitto *et al.* [32] noted that the valence band of high-spin Co^{2+} oxides with octahedrally coordination were more complex in case of CoO than in Co_3O_4, which should have more lines due to formal presence of Co^{2+} and Co^{3+}. The difference is, the high-spin oxides reveal effects not present in low-spin oxides: octahedrally coordinated Co^{3+} or tetrahedrally coordinated Co^{2+}. The first effect is a charge-transfer from O 2p to Co 3d, which cause variable finals states in the photoemission mechanism. The second effect is a strong electron correlation leading to varying d-d coupling in a range of closely localized states. The observation state is also compatible with the value of molar Curie constant observed in magnetic measurements, which is characteristic of a Co^{2+} in the S = 3/2 (high spin) state.

The complex shape of O 1s spectra (Fig. 9) can be associated with the oxygen ions located in various crystallographic positions, which can be divided into two groups depends on bond length. In SiO_2 oxygen is connected to silicon with short bonds 1.6 Å, whereas in pyroxenes the bond lengths of the three sites O1, O2 and O3 are distributed between 1.6 Å (Si – O1, Si – O2, Si – O3) through around 2.2 Å (Co – O1, Co – O2, Ca – O1, Ca – O2) to over 2.6 Å (Ca – O3). Spectral line at around 531.1 eV having the biggest intensity for N2 sample can be connected with the composite [31] and be related to the longest bonds of Ca. The second line at around 532.9 eV can be related to the shortest bonds of Si. Additionally, it may correspond to the oxygen bonds at additional phases of SiO_2 [33], therefore its intensity becomes dominant for N3 and N4 composites. Moreover, the peak at about 529.2 eV could be the result of weakly absorbed oxygen O_2/OH^- or the surface states. The higher binding energy of the 532.9 eV line associated with SiO_2 is in agreement with the chemical shift of the Si K absorption line seen in XANES.

The Si 2p spectra consist of two peaks with binding energies of 102.3 eV and 102.9 eV which can be assigned to Si $2p_{3/2}$ and Si $2p_{1/2}$, respectively, of Si^{4+} in $CaCoSi_nO_{2n+1}$ ceramics [31]. Additional spin-orbital doublet on the side of higher binding energy at around 103.5 eV for Si $2p_{3/2}$ and 104.1 eV for Si $2p_{1/2}$ for N3 and N4 composites can be connected to Si bonds in SiO_2 [34]. Binding energy of 347.4 eV for Ca $2p_{3/2}$ and 351 eV for Ca $2p_{5/2}$ reveals a divalent oxidation state for calcium [31].

Moreover, the deconvolution revealed the existence of the contributions from additional lines on the lower binding energy side which could be connected to surface states or various defects of ceramic structure. In case of N3H and N4H samples, where they are more visible, we cannot exclude a presence of additional phases, which are not detected by XRD, for example glasses. These extra lines of Si 2p and Ca 2p are not observed in the N2L (htx2) ceramics. This indicates better quality of the crystal structure of the N2L and may suggests that in the investigated samples, defects due to deviation from stoichiometry probably play a major role in charge compensation.

The sample structures of valence bands of $CaCoSi_nO_{2n+1}$ ceramics are shown in Fig. 10. The XPS spectra were normalized to the edges of the valence bands. According to the DFT electronic structure calculations in a range of about 2–8 eV they are mostly consist of the O 2p and Co 3d hybridized states. Moreover, the shape of the valence band exhibits the O 2p nonbonding orbital at binding energy about 5 eV at the valence band top and the states with dominating character Co 3d at binding energy about 7 eV weakly hybridized with O 2p states. The shape of the valence band in the range 6–18 eV is connected mainly with the hybridized states O 2p with Si 2p and Si 2 s [35,36] and the intensity of the valence band increases for N3 composition. Additionally, the spectra properties at around 16 eV may be the result of contamination (states C 2s and C 3p). The arrow in Fig. 10 points towards a half on the energy gap, so the energy gap estimated from the XPS measurements is about 4.4 eV for $CaCoSi_nO_{2n+1}$ ceramics with the Fermi level mid-way in the gap width. This value is compliant with results of electronic structure calculations.

3.5. *X-ray Absorption Near Edge Spectroscopy*

The prepared samples had a total absorption, μd < 3.5 with an edge step, Δμd from 0.7 to 1.7. Fig. 11 presents normalized Si K absorption edges of the selected samples. The edge positions E_0 calculated as the maximum of the first derivative of the signal were Si 1839.9 eV, SiO_2 am. 1847.3 eV, N2H (glazed) 1846.8 eV, N2L (htx2) 1846.8 eV, N3H (htx2) 1846.7 eV.

The position of the edges of the oxides and pyroxenes is shifted by about 7 eV towards higher energies, which agrees with their cationic character. The edge of the amorphous a-SiO_2 has even more cationic character with additional shift of 0.5 eV vs pyroxene.

The shape of the near edge region of the Si K edge reflects density of unoccupied electron states with symmetry dictated by the dipole electric transition rules Δl = ± 1. For the K edge, the initial state has an s-like symmetry, therefore the final states can only come from the p-like DOS

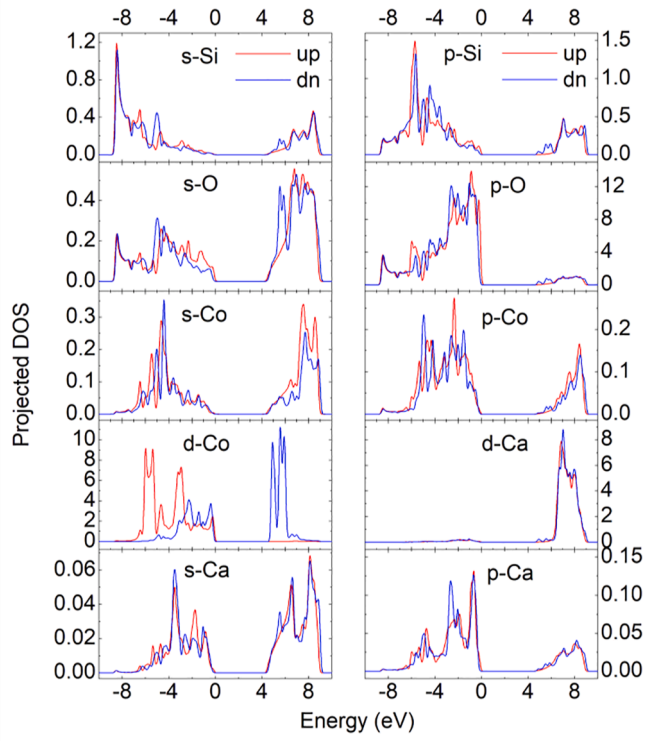

Fig. 12. Site and s, p, d-like projected densities of states for $CaCoSi_2O_6$. Labels "up" and "dn" denote spin-up and spin-down components.

around Si ion. Their electronic origin will be discussed below in the numerical section. The characteristic feature of all oxide edges is a pronounced white line (A). The highest amplitude is observed for N2L (htx2) and N2H (htx1) glazed, which in principle represent the same stoichiometry $CaCoSi_2O_6$. The difference between these two samples lies in two areas. N2L is phase pure and long range ordered while the N2H most likely contains $Ca_2CoSi_2O_7$, which explains its blue color and is glazed, therefore more glass-like. The glassy character of N2H versus crystalline H2L can be seen from the lack of the feature (B) located at about 1857 eV, which is clearly pronounced in crystalline N2L, N3H but suppressed in N2H. This feature is also not present in the amorphous SiO_2 despite formally the same first coordination shell.

The difference between the edges of crystalline N2L and N3H is limited to a lower amplitude of features (A) and (B) which comes from the increased content of the SiO_2 in the N3H sample.

3.6. Numerical calculations

$CaCoSi_2O_6$ was modeled using the crystal structure. Structure optimization was achieved using the VASP package [37]. The spin-polarized density functional theory (DFT) calculations were carried out within the generalized gradient approximation using the Perdew, Burke and Ernzerhof (PBE) functional [38]. The reciprocal space was sampled according to Monkhorst-Pack scheme with a k-point mesh of (12,12,12). The LDA + U functional was parametrized with U = 7 eV and J = 0.9 eV. The calculations were performed in a ferromagnetic configuration. Fig. 12 presents spin projected Densities of States (DOSes) of all elements in energy range between −10 eV and 10 eV, where 0 eV is located at the highest occupied electron state. A calculated band gap was equal to 4.4 eV. Calculated magnetic moments were equal to the dominant 2.85 μ_B on Co d-like DOS and negligible 0.03 μ_B on p-like DOS of Si.

4. Conclusion

Structural studies revealed that compositions with n = 3 and n = 4 are chemically dual (at least) phase mixtures of $CaCoSi_2O_6$ and the excess of SiO_2. The lack of these phases, at least in a form isostructural to the copper systems, can be understood in the following way. In the copper-based materials with n = 3 and n = 4, the transition metal ions are coordinated in a flat square way by oxygen, which is compatible with copper but not compatible with cobalt. Therefore, such possibility can be excluded. At the same time, it does not exclude other structures but so far, they have not been found.

The excess of SiO_2 suppresses formation of $Ca_2CoSi_2O_7$ (detected in XRD and SQUID data) and possibly Co_2SiO_4 (seen only in SQUID), which changes the color of the material from deep pink to bluish hue. Therefore, a slight excess of SiO_2 (<4%) might be added during the synthesis of the $CaCoSi_2O_6$ to get rid of the magnetic impurities.

Additionally, good homogenization by ball milling deceases the content of parasitical phases and allows to obtain pure material after the second heating.

The electronic structure on the good quality $CaCoSi_2O_6$ material studies by the XPS and the Si K XANES revealed that the silicon in a rigid tetrahedron is not a passive spacer but it is responding to the chemical environment. The chemical shift of the Si K edge changes between SiO_2, $CaCoSi_2O_6$ and $Ca_2CoSi_2O_7$ due to hybridization with the oxygen states, which also can be located in the VB-XPS at the bottom of the band.

Declaration of Competing Interest

The authors declare that they have no known competing financial interests or personal relationships that could have appeared to influence the work reported in this paper.

Acknowledgements

The research leading to these results received funding from the European Community Horizon 2020 research and innovation program under the grant agreement N. 730872 project CALIPSOPlus.

References

[1] H. Davy, Phil. Trans. R. Soc. Lond. 105 (1815) 97–124, https://doi.org/10.1098/rstl.1815.0009.
[2] A. Fores, M. Llusar, J.A. Badenes, J. Calbo, M.A. Tena, G. Monros, Green Chem. 2 (2000) 93–100, https://doi.org/10.1039/b000748j.
[3] M. Dondi, R.A. Eppler, Ullmann's Encyclopedia of Industrial Chemistry 1, Wiley-VCH Verlag GmbH & Co., KGaA, 2014.
[4] T. Mimani, S. Ghosh, Curr. Sci. 78 (2000) 892–896.
[5] E. Ozel, H. Yurdakul, S. Turan, M. Ardit, G. Cruciani, M. Dondi, J. Eur. Ceram. Soc. 30 (2010) 3319–3329, https://doi.org/10.1016/j.jeurceramsoc.2010.08.013.
[6] Available from: <https://www.lme.com/en-GB/Metals/Minor-metals/Cobalt#tabIndex=2> (accessed July 9th 2021).
[7] German Patent, 2002. Available from: <http://www.freepatentsonline.com/DE10121871.html> (accessed July 9th 2021).
[8] L. Mantovani, M. Tribaudino, M. Dondi, C. Zanelli, Dyes Pigments 120 (2015) 118–125, https://doi.org/10.1016/j.dyepig.2015.04.001.
[9] G. Durand, S. Vilminot, P. Rabu, A. Derory, J.P. Lambour, E. Ressouche, J. Solid State Chem. 124 (1996) 374–380, https://doi.org/10.1006/jssc.1996.0252.
[10] B.C. Chakoumakos, J.A. Fernandez-Baca, L.A. Boatner, J. Solid State Chem. 103 (1) (1993) 105–113, doi: 10.1006/jssc.1993.1083.
[11] H. Berke, Chem. Soc. Rev. 36 (2007) 15–30, https://doi.org/10.1039/b606268g.
[12] G. Accorsi, G. Verri, M. Bolognesi, N. Armaroli, C. Clementi, C. Miliani, A. Romani, Chem. Commun. (2009) 3392–3394, https://doi.org/10.1039/B902563D.
[13] D. Johnson-McDaniel, C.A. Barrett, A. Sharafi, T.T. Salguero, J. Am. Chem. Soc. 135 (2013) 1677–1679, https://doi.org/10.1021/ja310587c.
[14] Y. Chen, M. Kan, Q. Sun, P. Jena, J. Phys. Chem. Lett. 7 (2016) 399–405, https://doi.org/10.1021/acs.jpclett.5b02770.
[15] K. Hagiya, M. Ohmasa, K. Iishi, Acta Cryst. B 49 (1993) 172–179, https://doi.org/10.1107/S0108768192008048.
[16] M. Akaki, J. Tozawa, D. Akahoshi, H. Kuwahara, J. Phys.: Conf. Ser. 150 (2009), 042001, https://doi.org/10.1088/1742-6596/150/4/042001.
[17] M. Akaki, H. Iwamoto, T. Kihara, M. Tokunaga, H. Kuwahara, Phys. Rev. B 86 (2012), https://doi.org/10.1103/PhysRevB.86.060413.
[18] H. Murakawa, Y. Onose, S. Miyahara, N. Furukawa, Y. Tokura, Phys. Rev. Lett. 105 (2010), 137202, https://doi.org/10.1103/PhysRevLett.105.137202.
[19] S. Ghose, C. Wan, F.P. Okamura, Am. Mineral. 72 (1987) 375–381.
[20] G.J. Redhammer, G. Roth, W. Treutmann, W. Paulus, G. Andre, C. Pietzonka, G. Amthauer, J. Solid State Chem. 181 (2008) 3163–3176, https://doi.org/10.1016/j.jssc.2008.08.014.

[21] M. Chen, B. Hallstedt, L.J. Gauckler, J. Phase Equilib. 24 (3) (2003) 212–227, doi: 10.1361/105497103770330514.
[22] S. Nomura, R.P. Santoro, J. Fang, R.E. Newnham, J. Phys. Chem. Solids 25 (1964) 901–905, https://doi.org/10.1016/0022-3697(64)90104-0.
[23] J. Rodriguez-Carvajal, Recent developments of the program FULLPROF, in commission on powder diffraction (IUCr), Newsletter 26 (2001) 12–19.
[24] S. Doniach, M. Sunjic, J. Phys. C: Solid State Phys. 3 (2) (1970) 285–291.
[25] A. Balerna, Condens. Matter 4 (2019) 7, https://doi.org/10.3390/condmat4010007.
[26] A. Balerna, M. Cestelli Guidi, R. Cimino, M. Commisso, A. De Sio, L. Gambicorti, A. Grilli, D. Hampai, E. Pace, M. Pietropaoli, A. Raco, V. Sciarra, V. Tullio, G. Viviani, AIP Conf. Proc. 1234 (2010) 285–288; Experimental setup is available from <http://dafne-light.lnf.infn.it/>.
[27] Center for X-Ray Optics ALS, X-Ray Data Booklet 2009. Available from: <http://xdb.lbl.gov/>.
[28] H.M. Rietveld, J. Appl. Cryst. 2 (1969) 65–71, https://doi.org/10.1107/S0021889869006558.
[29] A. Sazonov, M. Meven, V. Hutanu, G. Heger, T. Hansen, A. Gukasov, Acta Cryst. B 65 (2009) 664–675, https://doi.org/10.1107/S0108768109042499.
[30] C.A.F. Vaz, D. Prabhakaran, E.I. Altman, V.E. Henrich, Phys. Rev. B 80 (2009), 155457, https://doi.org/10.1103/PhysRevB.80.155457.
[31] I. Michailova, D. Mehandjiev, Can. J. Chem. 89 (8) (2011) 939–947, doi: 10.1139/v11-061.
[32] S.C. Petitto, E.M. Marsh, G.A. Carson, M. Langell, J. Mol. Catal. A: Chem. 281 (2008) 49–58, https://doi.org/10.1016/j.molcata.2007.08.023.
[33] Available from: <https://xpssimplified.com/elements/oxygen.php> (accessed July 9th 2021).
[34] Available from: <https://xpssimplified.com/elements/silicon.php> (accessed July 9th 2021).
[35] A. Sobczak, R. Nietubyć, J.W. Sobczak, Acta Phys. Pol. A 86 (5) (1994) 837–843.
[36] M. Tallarida, K. Karavaev, D. Schmeisser, ECS Trans. 25 (4) (2009) 253–261, doi: 10.1149/1.3205060.
[37] G. Kresse, J. Furthmüller, Comput. Mater. Sci. 6 (1996), 15-50; G. Kresse, J. Furthmüller, Phys. Rev. B 54 (1996) 11169–11186, doi: 10.1103/physrevb.54.11169.
[38] J.P. Perdew, K. Burke, M. Ernzerhof, Phys. Rev. Lett. 77 (1996) 3865–3868, https://doi.org/10.1103/PhysRevLett.77.3865.